Title

Two-dimensional mapping of residual stresses in a thick dissimilar weld using contour method, deep hole drilling, and neutron diffraction

Journal

Journal of Materials Science, 51(23)

ISSN

0022-2461

Authors

Woo, Wanchuck
An, Gyu Baek
Truman, Christopher E
et al.

Publication Date

2016-12-01

DOI

10.1007/s10853-016-0283-z

Residual stress determination through the thickness of a thick dissimilar weld using neutron diffraction, deep hole drilling, and contour method

Wanchuck Woo [a], Gyu Baek An [b]*, Wenchun Jiang [c], Dong-Kyu Kim [a], Christopher Truman [d], and Michael R. Hill [e]

[a] *Neutron Science Division, Korea Atomic Energy Research Institute, Daejeon, 34057, South Korea*

[b] *Department of Naval Architecture & Ocean Engineering, Chosun university, Gwangju, 61452, South Korea*

[c] *College of Chemical Engineering, China University of Petroleum, Qingdao, 266555, PR China*

[d] *Department of Mechanical Engineering, University of Bristol, Bristol, BS8 1TR, UK*

[e] *Department of Mechanical and Aerospace Engineering, University of California, Davis, CA 95616, USA*

***Corresponding Author:**

Gyu-beak An

Department of Naval Architecture & Ocean Engineering,

Chosun University, Gwangju, 61452, South Korea

Phone: 82-62-230-7210

Fax: 82-10-6790-1204

E-mail: gyubaekan@chosun.ac.kr

(Manuscript to be submitted to: *Materials Science and Engineering A*)

[*]Author to whom correspondence should be addressed; electronic mail:gyubaekan@chosun.ac.kr

Abstract

Through-thickness variations of residual stresses were determined in a 70-mm thick dissimilar weld specimen consisting of ferritic steel base and austenitic steel weld metals. Neutron diffraction measurements were performed at different locations from the weld centerline and compared to the results of the deep hole drilling technique, which eliminates microstructure induced complexities such as a strong texture and large grain sizes. The contour method was utilized to provide two-dimensional maps of the longitudinal residual stress and confirmed the maximum stress locations and magnitudes. Significant tensile stresses (about 90% of yield strength) occur along the interface between weld and base metals near the top surface (about 15% of the depth). It is attributed to the large difference (5.8×10^{-6} 1/°C) in the coefficient of thermal expansion (CTE) between ferritic and austenitic steels. Finally, the maximum residual stresses were addressed as a function of the CTE based on finite element simulations.

Keywords: Residual stress, Neutron diffraction, Contour method, Deep hole drilling, Dissimilar weld

1. Introduction

Most of the penetration nozzle components, steam generator systems, and large diameter pipelines in power plants and pressure vessel industries require dissimilar metal welds between ferritic and austenitic steels [1,2]. Although the dissimilar welds are widely used in many engineering structures, there are limitations and difficulties to predict the localized physical, mechanical properties, and microstructures due to the inhomogeneous nature of the mixture [3-5]. In particular, it is critical to determine the location and magnitude of residual stresses in the dissimilar welds because serious cracking has been often initiated in the transition zone combined with the applied loading and degraded material properties under extreme operating conditions [6,7]. It is the case of the primary water stress corrosion cracking (PWSCC) in nuclear power plants. The high susceptibility to the PWSCC of the dissimilar welds can cause a preferred crack growth and abrupt fracture of the components [8,9].

A number of studies have been performed to determine the residuals tresses in the dissimilar welds based on computational simulation [10-16] and experimental methods [17-21]. Deng *et al*. predicted significant hoop stresses (over 140% of the yield strength of the weld metal) on the inside dissimilar welded pipe due to the large coefficient of thermal expansion (CTE) of the austenitic weld consumable (9.6Ni-19.9Cr-Fe bal.) [11]. Yaghi *et al*. reported that the residual stresses were developed near the top surface in both the weld and the heat-affected zone (HAZ) of a 30 mm thick dissimilar weld having two halves of ferritic steel pipes filled with an austenitic weld metal (1.48Fe-21.9Cr-Ni bal.) [14]. Eisazadeh *et al*. suggested that the primary role on residual stress formation is the CTE rather than the yield strength, thermal conductivity, specific heat capacity in ferritic and austenitic (8Ni-18Cr-Fe bal.) dissimilar welds by systematic modeling studies [16].

Several experimental approaches have been complemented with simulations even though mainly focused on the residual stresses of the PWSCC (ferritic to austenitic steel pipe joints with Ni-base alloy type weld metals) in nuclear power plant applications [17-21]. Joseph *et al*. measured residual stresses in 2.25Cr-1Mo ferritic steel and AISI 316 stainless steel pipes with and without Inconel 82 buttering using the x-ray diffraction [17]. Kim *et al*. and Woo *et al*. determined residual stresses in SA508 ferritic steel and 316L stainless steel pipes and its overlaid structures using x-day/hole drilling and neutron diffraction, respectively [18,19]. Ogawa *et al.* applied the deep hole drilling technique for the large scale (883 mm outer diameter) reactor vessel outlet nozzle to incorporate the residual stress distributions and the stress intensity factor in the heavy-section structures [20]. Olson *et al.* recently reported extensive results from a full size nozzle (375 mm long and 35 mm thick) dissimilar weld by using the slitting, hole drilling, and neutron diffraction methods [21]. At this moment, it is important to measure the variations of residual stresses through the thickness of the dissimilar weld plate without any geometrical complexities. Furthermore, in order to elucidate the influence of the CTE difference on residual stresses, it is necessary to prepare a specially designed ferritic to austenitic steel thick welding structure where the transient stresses can fully developed along the interface during the multi-pass welding procedure.

In this paper, we present: (i) spatial variations of macroscopic residual stresses through the thickness of a 70 mm thick dissimilar weld specimen measured by three different methods (neutron diffraction, contour method, and deep hole drilling); (ii) comparison of the through-thickness stress distributions between the conventional similar weld (ferritic to ferritic) and the dissimilar weld (ferritic to austenitic) specimens; and (iii) importantly the relationship between the CTE and the maximum tensile residual stress.

2. Processing, Microstructure, and Mechanical Properties

The base metal is the commercial high-strength low-carbon steel (wt% 0.05C, 0.1Si, 1.2Mn, 0.01P, and balance Fe) called EH40-TMCP. The average grain size was ~20 μm obtained by the typical hot rolling at ~ 1150 °C and water quenching to 500 °C followed by air cooling to room temperature. Two ferritic steel plates (each 600-mm long by 150-mm wide by 70-mm thick) were joined with an austenitic weld metal using the multi-pass flux cored arc welding technique, Fig. 1(a). The austenitic weld metal was specially designed for the no phase transformation, Table 1. The specimen was welded using a heat-input of 1.7 kJ/mm using a welding current, voltage, and electrode speed of 255 A, 32 V and 5 mm/s, respectively. The macroscopic structure is shown in Fig. 2 with cross-sections extracted from the plates. The welding process provided a bead width of about 60 mm on the top surface after 61 passes, with 21 layers welding in a groove of 30°, as shown in Fig. 2.

After welding, the dissimilar weld plate was cut slowly into two parts with the dimensions of 280 mm length (discard each edge of 20 mm) and 300 mm width by using a band saw, as shown in Fig. 1(a). Each cut plate was provided for the residual stress measurements using neutron diffraction and deep hole drilling/contour method, respectively. In the remainder of the paper x, y, and z directions denote longitudinal (welding), transverse, and normal directions, respectively, as shown in Fig. 1(a). Microstructural characterization was performed on the cross-section of the weld, Fig. 2. The locations for the optical microscopy were 5, 35, 65 mm from the top surface along the weld centerline as marked by three squares. The microstructure of the weld metal reveals a strong grain orientation due to the elongated grains along the z direction of the weld. Besides, the grain size is mostly over 200 μm at the face and center weld regions. Note that the strong texture and large grain size can cause significant errors or unavailability in diffraction of the ND experiments.

Tensile specimens were machined from the base and weld metals at the mid-thickness with the gage length parallel to the longitudinal direction (x). Following the ASTM E 8M-04

procedure the dimension of the tensile specimen was 6.25 mm diameter and 32 mm long in the gage section. The specimens were prepared using electrical-discharge machining (EDM) and tensile tests were performed at room temperature using a constant crosshead velocity providing an initial strain rate of 6.7 x 10^{-4} s^{-1}. The yield and tensile strengths of the base metal were 410 and 520 MPa and those from the weld metal were 460 and 630 MPa, respectively, as shown in Fig. 3(a) and Table 2. Thermal dilation experiments were performed using samples of 4 mm in diameter and 10 mm in length cut by EDM from the base and weld metals. Thermal expansion and contraction were recorded during heating to 1150 °C at a rate of 10 °C/s, holding for 5 min, and cooling down to room temperature at a rate of 10 °C/s. The dilatometer test provides the CTE as 12.6 (1/°C, x10^{-6}) for the base metal and 18.4 (1/°C, x10^{-6}) for the austenitic weld metal by analysis of the linear expansion from room temperature to 100 °C. No phase transformation was clearly observed in the austenitic weld metal during heating and cooling. Vickers microhardness (Hv) was measured 15 times at each location from the weld centerline of 0, 30, 60, and 100 mm, and 15-mm below the top surface.

3. Residual stress measurements and simulation methods

3.1. Neutron diffraction, contour method, and deep hole drilling

Three methods of residual stress measurement were used in this work: neutron diffraction (ND), the contour method (CM) and deep hole drilling (DHD). ND has become a well-established method for measuring macroscopic residual stresses in the interior of polycrystalline [22]. Spatially-resolved neutron strain scanning was performed by using the Residual Stress Instrument (RSI) at Korea Atomic Energy Research Institute (KAERI) [23]. The wavelength selection methodology, which minimized the total cross-section and enhance the neutron beam attenuation, enable us to measure the residual stresses through the thickness

of the 70-mm thick weld, Fig. 4 [24]. Wavelengths of 2.39 Å were selected for the diffraction planes (110) for the bcc ferritic base metal and (111) for the fcc austenitic weld metal at scattering angles of 71.4° and 72.0°, respectively. The nominal scattering volumes of 4(x) × 8(y) × 4(z) mm^3 for the diffraction patterns with their scattering vectors were configured to be parallel to the x direction and a volume of 20(x) × 4(y) × 4(z) mm^3 for the y or z directions. A total of 13 points were measured through the thickness starting from 5 mm from the top surfaces to 65 mm in 5 mm steps at locations from the weld centerline of 0, 30, 60, and 100 mm, as shown in Fig. 1. Mostly, the measurement period was about 1 hour for each strain component achieving a strain uncertainty of about ±100 με.

Diffraction peaks were analyzed using a least squares Gaussian fitting method in the RSI data analysis program. Once the peak position was determined, the elastic lattice strains (ε) were calculated using $\varepsilon=-cot\theta(\theta-\theta_o)=(d-d_o)/d_o$, where the θ_o (d_o) and θ (d) are the diffraction angles (d-spacings) for the stress-free and stressed materials at each position, respectively [22]. The generalized Hooke's law was used to convert elastic strains (ε_x, ε_y, ε_z) to the residual stresses (σ_x, σ_y, σ_z) along the three orthogonal directions (x, y, and z) in a given plate. The used diffraction elastic constants and Poisson's ratios were E_{111} of 247.9 GPa, ν_{111} of 0.24 for the austenitic weld metal (0 mm location) and E_{110} of 225.5 GPa, ν_{110} of 0.28 for the ferritic base metal (30, 60, and 100 mm locations) [22]. Comb-like "stress free" reference samples were extracted along each line of strain scanning as shown in Fig. 1(a). The combs were 10 mm long (x), 4 mm wide (y), and 5 mm deep (z), Fig. 1(d). The stress-free lattice spacing (d_o) was carefully measured with the gauge volume was 8 mm^3 (2 x 2 x 2 mm^3).

Secondly, the deep hole drilling (DHD), a mechanical strain relief technique for measuring residual stresses [24], was performed at the weld centerline (0 mm), Fig. 1(a). The longitudinal (σ_x) and transverse (σ_y) stress components were calculated via the distortions of a reference hole created through the thickness of interest, Fig. 1(c). Note that the incremental

DHD (iDHD), which utilizes repeated hole-diameter measurements in each incremental machining step, is applied for the high magnitude of the plastic relaxation from 20 to 50 mm depth during the standard DHD process. A number of stress data obtained along the depth profile at weld centerline can supplement the ND results. Finally, the contour method (CM) was applied to determine residual stresses over a cross-section by measuring displacements of an EDM cut surface with a 100 μm diameter brass wire, Fig. 1(b). The displacements occurred due to the relaxation of the internal stress are compared to an assumed flat surface contour and the longitudinal (σ_x) residual stresses are recreated using a finite element model. The forces required to ensure the measured deformed surface is returned to its original position represent the residual stresses. The method provides a two-dimensional map having a regular resolution of 0.5 x 0.5 mm of the residual stresses normal to the cut-surface. The used Young's modulus and Poisson's ratio were E = 219 GPa for the base metal and 184 GPa for the weld metal as summarized in Table 2.

4. Results

4.1. Residual stress measurements by using ND and DHD

The measured distributions of residual stresses are shown in Fig. 5 for the 70 mm thick ferritic-austenitic dissimilar steel welded specimens. Each figure shows the through-thickness variations of residual stresses through the four different measurement locations as shown in Fig. 1(a). The stress uncertainties were mostly less than ± 50 MPa. Overall stress profiles seem to be different between weld and base metals, Figs. 5(a) and (d), which were measured at 0 mm and 100 mm locations from the weld centerline, respectively. The weld (0 mm) and HAZ (30 mm), Figs. 5(a)-(b), show that the three profiles similarly fluctuate showing a sine-wave like distribution. Smith *et al.* reported a similar stress profile in the region adjacent to the heat-affected zone of 108 mm thick steel weld [25]. The variation of residual stresses

(±200 MPa) is not significant to the yield strength of the weld metal (460 MPa). Meanwhile, the stress profiles obtained at the 60 and 100 mm locations, Figs. 5(c)-(d), exhibit an "M" shape with the σ_x and σ_y in compression up to -400 MPa near the surfaces balanced with tension (~ 200 MPa) at depths of about 25 and 50 mm. These profiles are typical in hot-rolled and quenched thick steel plates [24].

Figure 5(a) shows residual stresses obtained from the DHD and iDHD measurements along the weld centerline of the dissimilar welded specimen, Fig. 1(c). It should be noted that the ND measurements are unavailable at a few locations (5, 10, 25, 30 mm depth) along the centerline due to the insufficient peak statistic from the austenitic weld metal caused by the strong texture and large grain size as shown in the face and the center of Fig. 2. In both measurements the σ_x shows higher magnitudes (up to 270 MPa) than σ_y at most depths excepting the distinct compression near the bottom (~65 mm). As a result the DHD results complement the ND results of the weld metal region within the difference of about ± 50 MPa, Fig. 5(a).

4.2. Two-dimensional distribution of residual stresses in the dissimilar thick weld

Figure 6(a) shows the two-dimensional map of the σ_x measured at the cross-section of the 70 mm thick dissimilar weld. It is constructed by the contour method (CM) with the uncertainty of about ± 30 MPa. Overall it shows high tensions near the weld metal balancing with compressions in the base metal. It should be mentioned that significant tensile stresses (up to 400 MPa, about 90% of yield strength) are distributed along the interface between austenitic weld and ferritic base metals. It is a distinct feature of the ferritic-austenitic dissimilar steel weld, Fig. 6(a), when compared to the conventional ferritic similar steel weld, Fig. 6(b), in ref. 24. Note that the welding parameters including heat inputs, welding passes, and geometries are similar of the two welds. Detail comparisons will be addressed in the

discussion section. Compressive residual stresses (-160 MPa) exist near the bottom side (55~70 mm) of the plate weld specimen to achieve the necessary stress balance through the thickness of the specimen resulting in an angular distortion of about 1° downward, Fig. 6(a) [26].

Figure 7 shows profiles of σ_x extracted from the CM mapping along the four through-thickness lines (at 0, 30, 60, and 100 mm) as marked in Fig. 6(a). The previous result of DHD was included with the gray line for comparison, Fig. 7(a). Overall trends for the CM profiles are similar to the ND results in the four locations, though CM can provide much higher spatial resolution (1 mm spacing) than ND (5 mm gauge volume) for data analysis. The scatters of ND results can be attributed to the inappropriate 'stress-free' reference specimens associated with microstructure changes and/or different spatial averaging among methods.

5. Discussion

5.1. Residual stress comparison between similar and dissimilar welds

Let us discuss first about the difference in residual stress distributions between the dissimilar (ferritic-austenitic) and similar (ferritic-ferrritic) steel welds, Figs. 6(a) and 6(b), respectively. In both specimens, significant amounts of tensile residual stresses (about 90% yield strength of the base metal) were measured. In terms of the location, however, the significant tensile stresses were found near to the weld centerline at the top surface of the similar weld, Fig. 6(b), due to the accumulated thermal expansion/contraction and non-uniform plastic flow during welding [27]. Meanwhile, those were distributed near the interface between the weld and based metals in the dissimilar weld, Fig. 6(a). It is clear when compared the stress profiles extracted from the maps across the 5 mm below the top surface, Fig. 6(c). Figure 8(a) represents the specific locations of the residual stresses above 328 MPa

(80% of yield strength) and shows the maximum residual stress (400 MPa) developed along the interface from 10 to 15 mm from the top surface.

A number of studies have been reported that the residual stresses are prevailed near the interface of the dissimilar weld case [10-21]. In general, it is considered that the relatively larger CTE with higher strain hardening rate (lower thermal conductivity and heat transfer rate) of the austenitic steel part induces higher tensile stresses after welding in dissimilar welds [15-17]. There is an argument, however, among the specific locations of the maximum stress suggesting at the austenite steel part [10,16,17], ferritic steel part [11,13,18,21], or both sides [14,15]. The location of the harmful tension is important because it can be critical to the crack initiation and fracture behavior of components [28]. Although the yield strength of the ferritic base metal (410 MPa) is lower than that of the austenitic weld metal (460 MPa), Table 2, higher stresses were found at the heat-affected zone toward the ferritic steel region as shown in Fig. 6(a). Such higher stressed region is likely due to the significant strain hardening experienced via repeated welding processes followed by the fast cooling induced hard, brittle bainite and/or martensite structures in the multi-pass thick welding structures [29]. Indeed, the microstructures along the interface and transition zone, Fig. 2, exhibit localized banitic, tempered martensitic microstructures. Furthermore, Fig. 8(b) shows relatively higher microhardness of the interface (HAZ 30mm) compared to other locations and the value of 210 H_v is reasonable for the tempered martensite in 0.05 wt% C steel [30].

5.2. Residual stress dependency on the coefficient of thermal expansion.

Various parameters including yield strength, hardening modulus, thermal conductivity, specific heat capacity and/or geometries of components have been known to affect residual stresses extensively in the dissimilar welds, [11,14]. Systematic modeling studies by Eisazadeh *et al*. suggested that the CTE is dominant to determine the residual stress

formation rather than the yield strength, thermal conductivity, specific heat capacity in ferritic and austenitic (8Ni-18Cr-Fe bal.) dissimilar welds [16]. Deng *et al.* [11] and Lee *et al.* [13] emphasized that the sufficient thermal stresses can be caused by the large CTE difference (ΔCTE) between low alloy steel and austenitic stainless steel. Through a simple calculation in the current dissimilar welds (ΔCTE of 5.8×10^{-6} 1/°C), the thermal strain (ε^{th}) can about 1700 με corresponding to 370 MPa once the weld cools down from 300 °C to room temperature during a series of multi-pass welding.

Figure 9 shows a correlation between the residual stress and the ΔCTE in the ferritic-austenitic steel dissimilar welds. Note that this figure was constructed by literatures and the current experimental data. The maximum residual stress was chosen and normalized by the yield strengths of each specimen. It shows a proportional relationship between the maximum stress and ΔCTE in the dissimilar welds though there is a variance as the ΔCTE increases. Relatively higher residual stresses were found in the pipe weld cases [10,11,15] than plate welds [13,16] plausibly due to the large circular constraints and bending moments in pipes. It reduced when the welding consumable uses the Inconel type alloys, which are designed to have the similar CTE of the Cr-Mo ferritic steel [14,17]. The current experimental data is located at low, which can be attributed to the relatively low heat-input (1.7 kJ/mm) and the tempering effect in the multi-pass welding of the 70 mm thick plate specimen.

6. Conclusions

1. Microstructure, longitudinal tensile properties, coefficient of thermal expansion (CTE), and residual stresses were extensively examined in 70 mm thick dissimilar weld specimens joined between the ferritic steel base metal and austenitic steel weld metal. The yield strengths of 410 and 460 MPa, and Young's modulus of 219 and 184 GPa were obtained in the base and weld metals, respectively. The CTE difference is 5.8×10^{-6} 1/°C. No phase transformation

was observed in the austenitic weld metal, whilst the martensitic phase prevailed near the interface between ferritic and austenitic steels resulting in the microhardness increases.

2. In order to obtain full-field knowledge of the magnitudes and spatial distributions of the residual stresses, three methods were applied. Neutron diffraction (ND) measurements were performed at the weld centerline (0mm) and 30, 60, and 100 mm locations from the weld centerline through the thickness of the specimen and compared to the results of the deep hole drilling (DHD) technique by eliminating microstructure-induced complexities. Finally the contour method (CM) was utilized to provide two-dimensional maps of the longitudinal residual stress and confirmed the maximum stress locations and magnitudes.

3. Significant amounts of tensile residual stresses (about 90% yield strength of the base metal) were measured near the interface between the weld and based metals in the dissimilar weld. The residual stress mapping elucidates that the maximum residual stress (400 MPa) was developed along the interface from 10 to 15 mm from the top surface (0.15~0.2 depth to thickness ratio).

Acknowledgements

This work was supported by the National Research Foundation of Korea (NRF) grant funded by the Korean government (MSIP:Ministry of Science, ICT and Future Planning) (No. NRF-2012M2A2A6004262). It is also supported by POSCO project No. 20156342. The authors would like to thank D. J. Smith, V. T. Em, A. T. DeWald, and E. J. Kingston for their help.

References

[1] J. Besson, Y. Madi, A. Mortarjemi, M. Kocak, G. Martin, P. Hornet, Mater. Sci. Eng. A 397 (2005) 84-91.

[2] K.D. Kenneth, in: Nuclear Engineering Handbook, CRC Press, Boca Raton, Taylor and Francis, 2009.

[3] V.V. Satyanarayana, G. Madhusudhan Reddy, T. Mohandas, J. Mater. Proc. Tech. 160 (2005) 128-137.

[4] J.W. Kim, K. Lee, J.S. Kim, T.S. Byun, J. Nucl. Mater. 384 (2009), 212-221.

[5] J. Hou, Q.J. Peng, Y. Takeda, J. Kuniya, T. Shoji, J.Q. Wang, E.-H. Han, W. Ke, J. Mater. Sci. 45 (2010) 5332-5338.

[6] C. Cheung, U. Erb, G. Palumbo, Mater. Sci. Eng. A 185 (1994) 39-43.

[7] G. Saji, Nuclear Eng. Des. 239 (2009) 1591-1613

[8] M. Karlik, I. Nedbal, J. Siegl, Mater. Sci. Eng. A 357 (2003) 423-428.

[9] C. Jang, P.Y. Cho, M. Kim, S.J. Oh, J.S. Yang, Mater. Design 31 (2010) 1862-1870.

[10] D. Akbari, I. Sattari-Far, Inter. J. Press.Vessel Piping 86 (2009) 769-776.

[11] D. Deng, K. Ogawa, S. Kiyoshima, N. Yanagida, K. Saito, Comp. Mater. Sci. 47 (2009) 398-408.

[12] T.-K. Song, J.-S. Kim, C.-Y. Oh, Y.-J. Kim, C.-Y. Park, K.-S. Lee, Fat. Frac. Eng. Mater. Struc. 34 (2011) 624-641.

[13] C.-H. Lee, K.-H. Chang, Appl. Therm. Eng. 45-46 (2012) 33-41

[14] A.H. Yagi, T.H. Hyde, A.A. Becker, W. Sun, Inter. J. Press. Vessel Piping 111-112 (2013) 173-186.

[15] C.-H. Lee, K.-H. Chang, J.-U. Park, Nuclear Eng. Des. 256 (2013) 160-168.

[16] H. Eisazadeh, A.Achuthan, J.A. Goldak, D.K. Aidun, J. Mater. Proc. Tech. 222 (2015) 344-355.

[17] A. Joseph, S.K. Rai, T. Jayakumar, N. Murugan, Inter. J. Press.Vessel Piping 82 (2005) 700-705.

[18] K.S. Kim, H.J. Lee, B.S. Lee, I.C. Jung, K.S. Park, Nuclear Eng. Des. 239 (2009) 2771-2777.

[19] W. Woo, V. Em, C.R. Hubbard, H.-J. Lee, K.S. Park, Mater. Sci. Eng. A 528 (2011) 8021-8027.

[20] N. Ogawa, I. Muroya, Y. Iwamoto, T. Ohta, M. Ochi, K. Hojo, K. Ogawa, Inter. J. Press. Vessel Piping 90-91 (2012) 84-90.

[21] M.D. Olson, M.R. Hill, B.Clausen, M.Steinzig, T.M. Holden, Exp. Mechanics 55 (2015) 1092-1103.

[22] M.T. Hutchings, P.J. Withers, T.M. Holden, T. Lorentzen, in: Introduction to the characterization of residual stress by neutron diffraction, 1st ed, London, Taylor and Francis, 2005.

[23] W. Woo, V. Em, B.S. Seong, E. Shin, P. Mikula, J. Joo, M.-H. Kang, J. Appl. Crystal. 44 (2011) 747-754.

[24] W. Woo, G.B. An, E.J. Kingston, A.T. DeWald, D.J. Smith, M.R. Hill, Acta Mater. 61 (2013) 3564-3574.

[25] D.J. Smith, P.J. Bouchard, D. George, J. Strain Analysis 35 (2000) 287-305.

[26] W. Woo, H. Choo, D.W. Brown, Z. Feng, P.K. Liaw, Mater. Sci. Eng. A 437 (2006) 64-69.

[27] Masubuchi K. Analysis of Welded Structures. New York: Pergamon; 1980.

[28] S.Y. Lee, P.K. Liaw, H. Choo, R.B. Rogg, Acta Mater 59 (2011) 495-502.

[29] J.N. DuPont, C.S. Kusko, Welding Research (2007) 51s-54s.

[30] R.K. Shiue, K.C. Lan, C. Chen, Mater. Sci. Eng. A 287 (2000) 10-16.

Table caption

Table 1. Chemical compositions of the dissimilar weld.

Table 2. Mechanical properties of the dissimilar weld.

Table 1

Element (wt. %)	C	Si	Mn	Ni	Cr	Fe
Base metal (ferritic)	0.05	0.1	1.2	-	-	bal.
Weld metal (austenitic)	0.03	0.3	0.52	12.3	12.1	bal.

Table 2

Material properties	Yield strength (MPa)	Tensile strength (MPa)	Young's modulus (GPa)	Poisson's ratio	Coefficient of thermal expansion* (x10^{-6}, 1/℃)
Base metal (ferritic)	410	520	219	0.28	12.6
Weld metal (austenitic)	460	630	184	0.31	18.4

Figure captions

Fig. 1. Schematic of the sample dimension, (a) measurement locations for the neutron diffraction (ND), contour method (CM), and deep hole drilling, (b) contour plane and constraint (arrows) on cutting, and (c) a cylindrical trepanned core, and (d) dimension of the reference combs for the "stress-free" lattice spacing (d_o) measurements.

Fig. 2. Cross-sectional macrostructure of the 70-mm thick ferritic-austenitic steel dissimilar weld specimen. Marked squares for optical micrographs and lines along the mid-thickness (*center*), 5 mm below the top (*face*), and 5 mm above the bottom (*root*).

Fig. 3. (a) Tensile test results of ferritic steel base metal and austenitic steel weld metal. Tensile specimens were taken along the longitudinal direction and (b) Thermal dilation experimental results. The coefficient of thermal expansion (CTE) is the linear expansion from room temperature to 100 ^oC in dilatometer tests. The M_s and M_f denote martensite starting and finishing temperature, respectively.

Fig. 4. Experimental set up for neutron-diffraction measurements.

Fig. 5. Residual stresses through the thickness of the dissimilar weld specimen using neutron diffraction; along (a) 0, (b) 30, (c) 60, and (d) 100 mm locations from the centerline. The DHD measurements along the longitudinal (σ_x) and transverse (σ_y) direction were was profiled as thick lines in Fig. (a).

Fig. 6. Two-dimensional mapping of the longitudinal residual stress (σ_x): (a) dissimilar weld and (b) similar weld [24] by using contour method (CM). (c) Stress profiles extracted from the maps across the 5 mm below the top surface, Figs. 6(a)-(b).

Fig. 7. Comparison of the longitudinal residual stress (σ_x) between the CM and ND; along (a) 0, (b) 30, (c) 60, and (d) 100 mm locations from the centerline. The DHD measurements were profiled as a thick grey line in Fig. (a).

Fig. 8. (a) A diagram representing residual stress locations. Marked stresses above 328 MPa and the maximum residual stress (400 MPa) and (b) microhardness results measured at (a) 0, (b) 30, (c) 60, and (d) 100 mm locations marked in Fig. 8(a).

Fig. 9. The maximum residual stresses as a function of the CTE difference (ΔCTE). Note that the stress is normalized by the yield strengths of each specimen and the numbers with parenthesis indicate references.

FIGURE 1

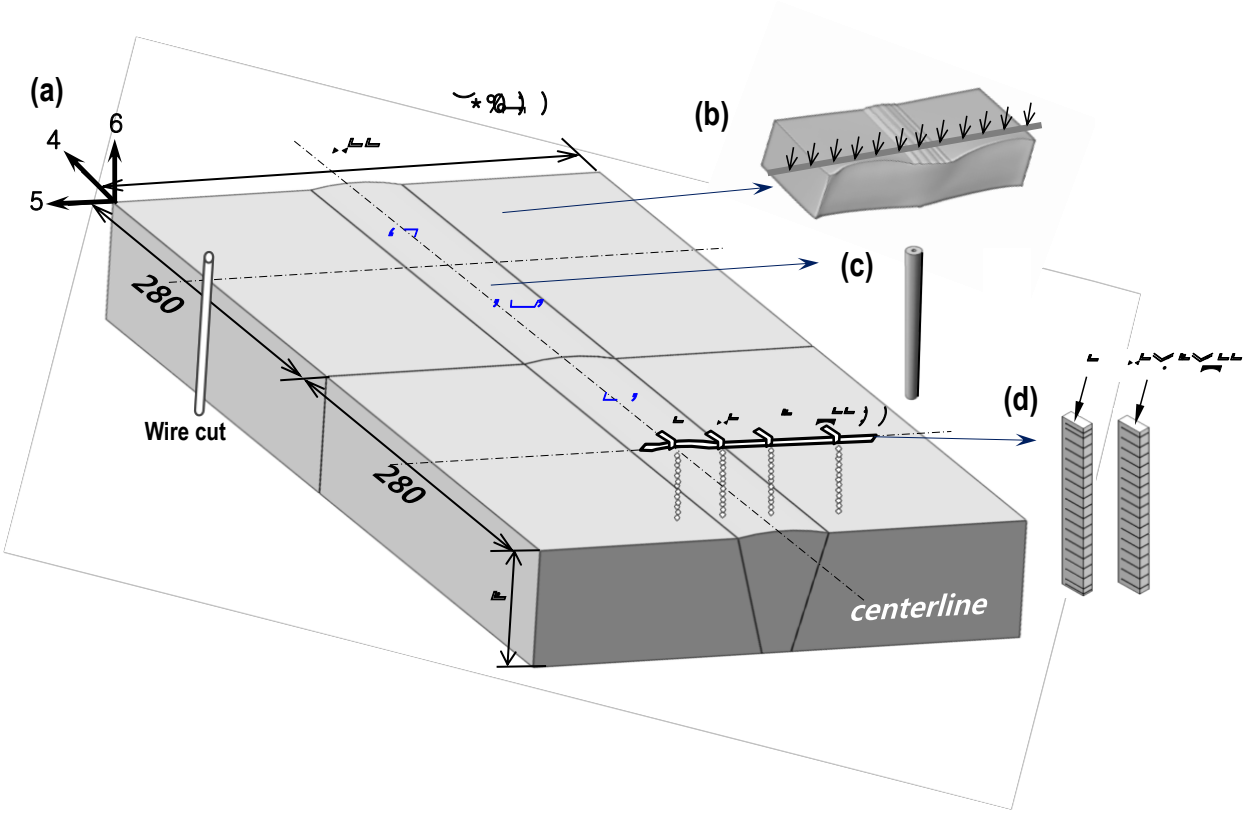

FIGURE 2

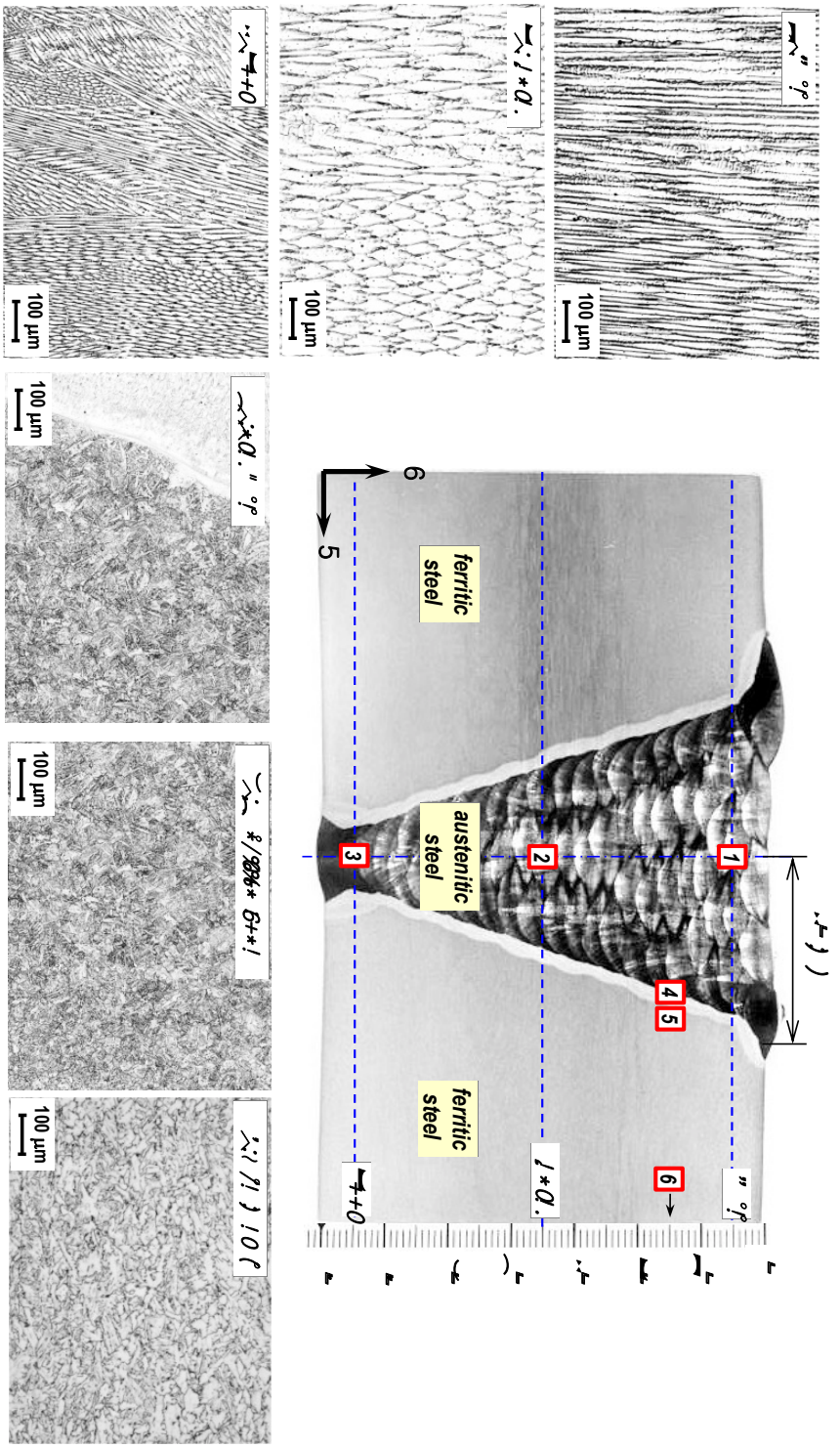
ferritic steel
austenitic steel
ferritic steel
1
2
3
4
5
6
100 µm

FIGURE 3

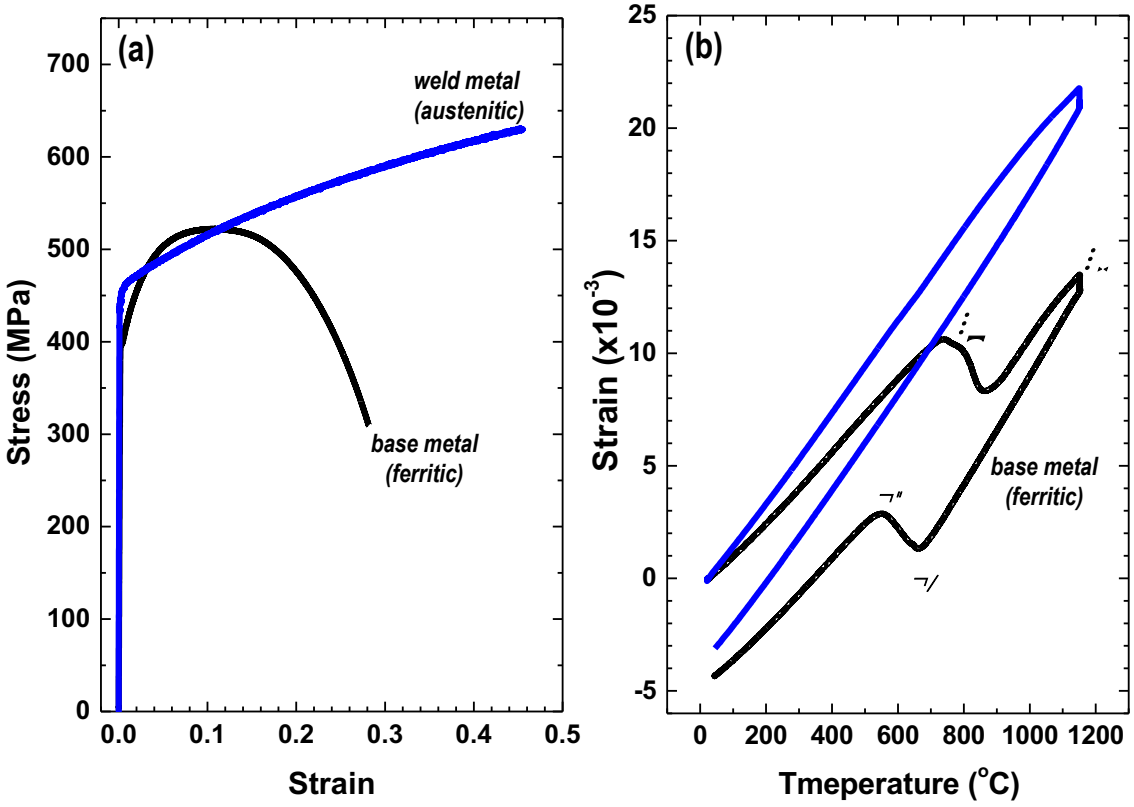
(a)
weld metal
(austenitic)
base metal
(ferritic)
Stress (MPa)
Strain
0
100
200
300
400
500
600
700
0.0
0.1
0.2
0.3
0.4
0.5
(b)
base metal
(ferritic)
Strain (x10-3)
Tmeperature (°C)
-5
0
5
10
15
20
25
0
200
400
600
800
1000
1200

FIGURE 4

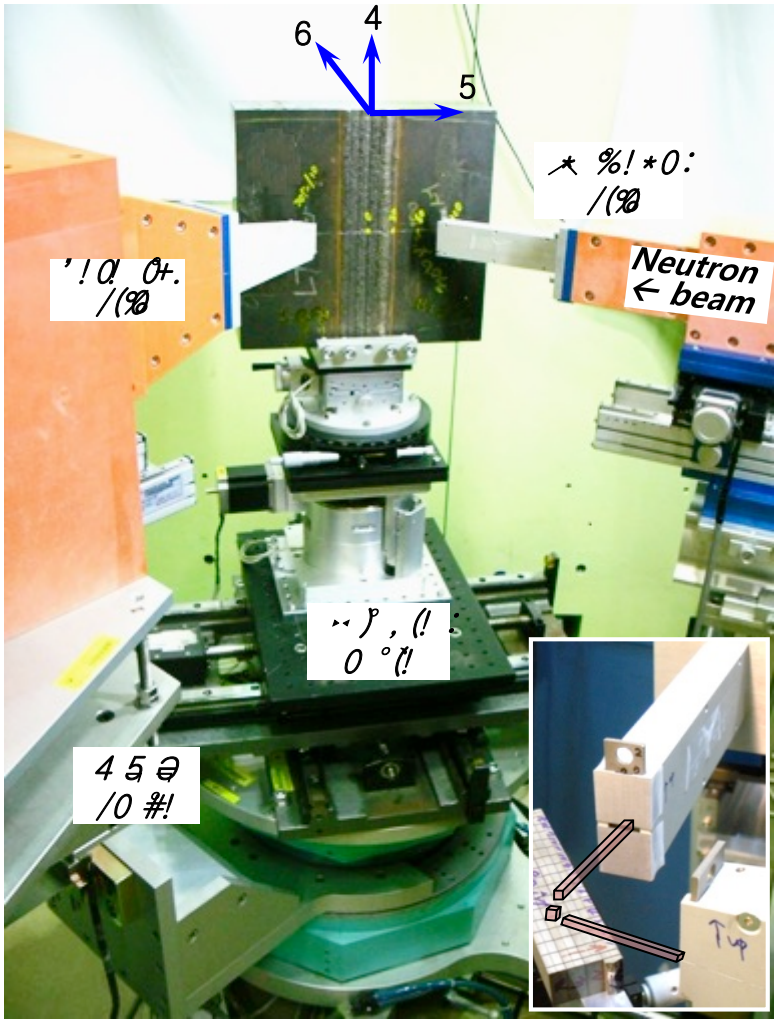

FIGURE 5

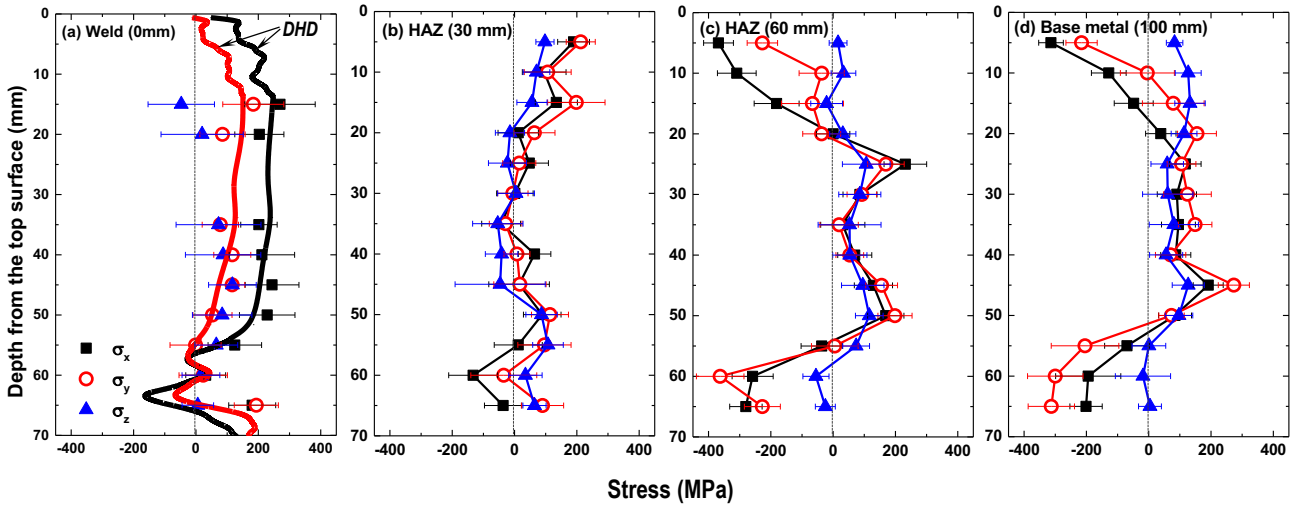
(a) Weld (0mm)
DHD
(b) HAZ (30 mm)
(c) HAZ (60 mm)
(d) Base metal (100 mm)
σx
σy
σz
Depth from the top surface (mm)
Stress (MPa)
0
10
20
30
40
50
60
70
-400
-200
0
200
400

FIGURE 6

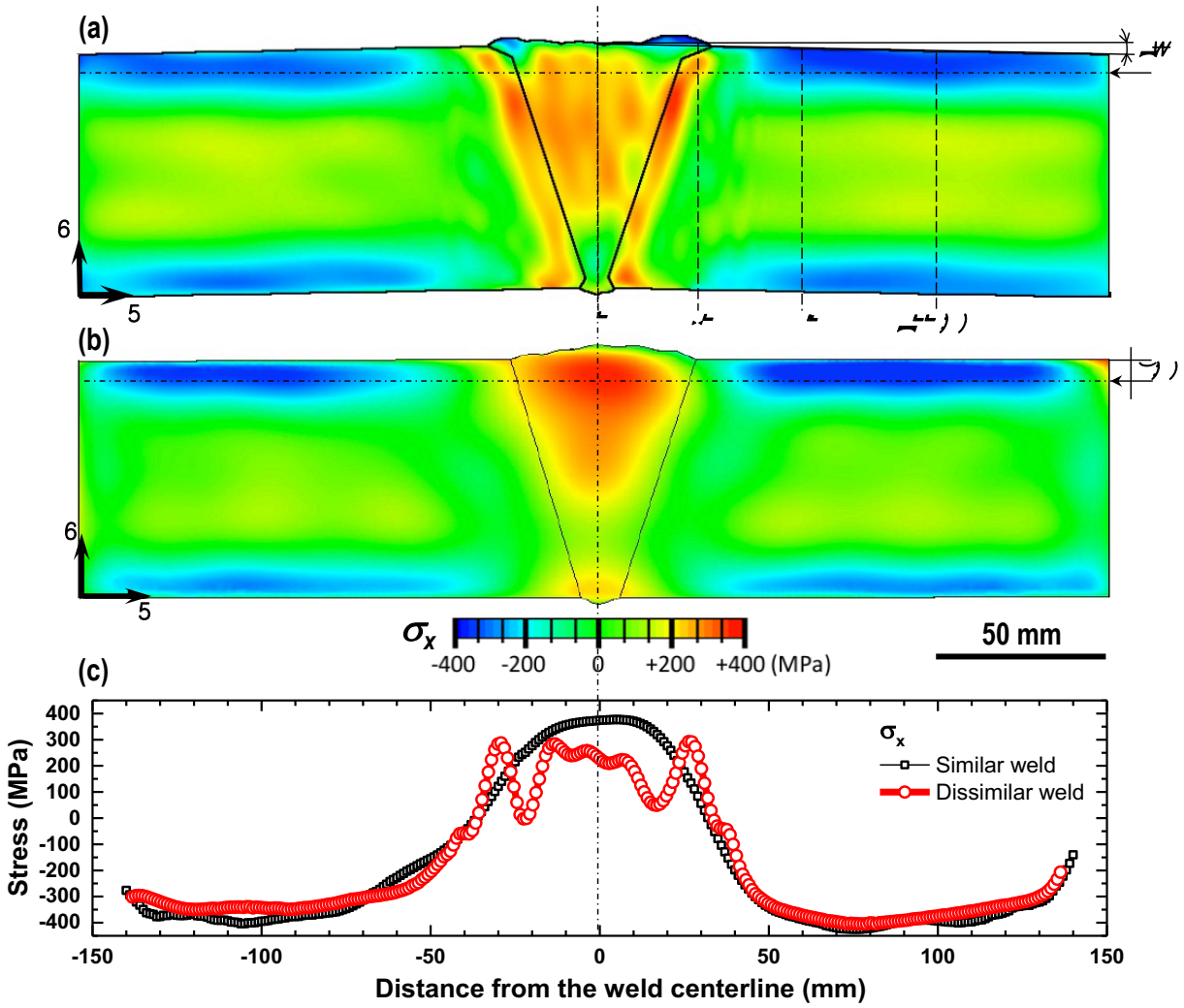
(a)
6
5
(b)
6
5
σx
-400 -200 0 +200 +400 (MPa)
50 mm
(c)
Stress (MPa)
400
300
200
100
0
-100
-200
-300
-400
-150 -100 -50 0 50 100 150
Distance from the weld centerline (mm)
σx
Similar weld
Dissimilar weld

FIGURE 7

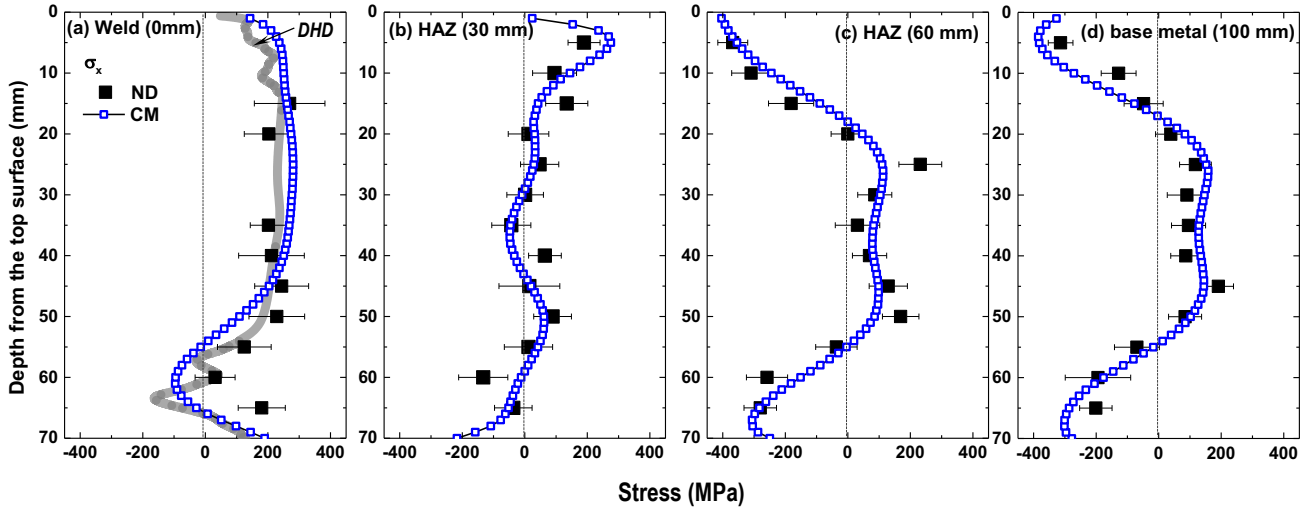
(a) Weld (0mm)
DHD
σx
ND
CM
(b) HAZ (30 mm)
(c) HAZ (60 mm)
(d) base metal (100 mm)
Depth from the top surface (mm)
Stress (MPa)
0
10
20
30
40
50
60
70
-400
-200
0
200
400

FIGURE 8

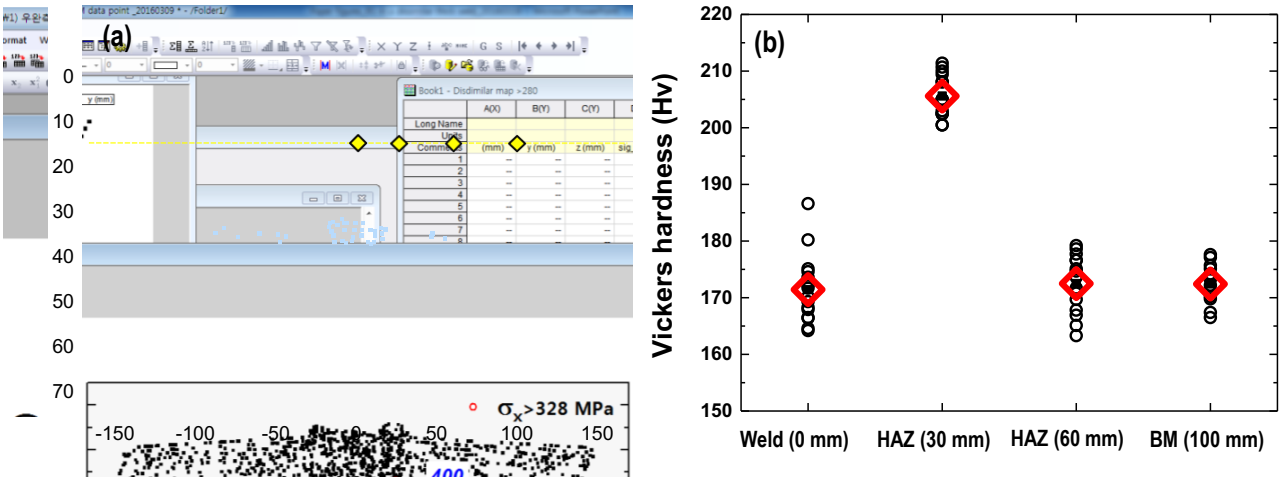
(a)
0
10
20
30
40
50
60
70
-150
-100
-50
0
50
100
150
σx>328 MPa
(b)
Vickers hardness (Hv)
220
210
200
190
180
170
160
150
Weld (0 mm)
HAZ (30 mm)
HAZ (60 mm)
BM (100 mm)

FIGURE 9

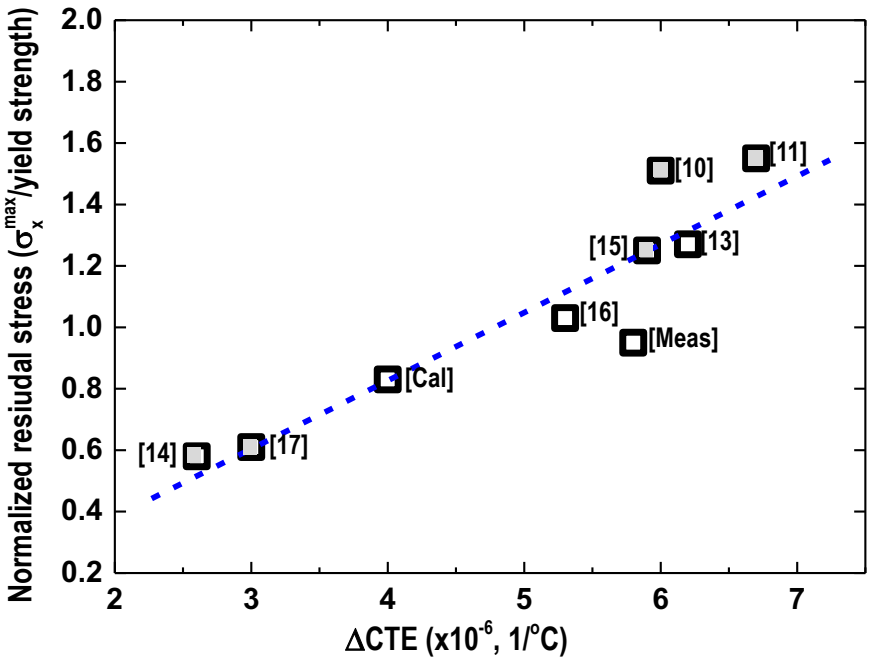
Normalized resiudal stress (σ_x^{max}/yield strength)
2.0
1.8
1.6
1.4
1.2
1.0
0.8
0.6
0.4
0.2
2
3
4
5
6
7
ΔCTE (x10^{-6}, 1/°C)
[10]
[11]
[15]
[13]
[16]
[Meas]
[Cal]
[14]
[17]